Multiple Fitness Peaks on the Adaptive Landscape Drive Adaptive Radiation in the Wild

Christopher H. Martin and Peter C. Wainwright

Science **339**, 208 (2013);
DOI: 10.1126/science.1227710

Science (print ISSN 0036-8075; online ISSN 1095-9203) is published weekly, except the last week in December, by the American Association for the Advancement of Science, 1200 New York Avenue NW, Washington, DC 20005.

Multiple Fitness Peaks on the Adaptive Landscape Drive Adaptive Radiation in the Wild

Christopher H. Martin* and Peter C. Wainwright

The relationship between phenotype and fitness can be visualized as a rugged landscape. Multiple fitness peaks on this landscape are predicted to drive early bursts of niche diversification during adaptive radiation. We measured the adaptive landscape in a nascent adaptive radiation of *Cyprinodon* pupfishes endemic to San Salvador Island, Bahamas, and found multiple coexisting high-fitness regions driven by increased competition at high densities, supporting the early burst model. Hybrids resembling the generalist phenotype were isolated on a local fitness peak separated by a valley from a higher-fitness region corresponding to trophic specialization. This complex landscape could explain both the rarity of specialists across many similar environments due to stabilizing selection on generalists and the rapid morphological diversification rate of specialists due to their higher fitness.

Adaptive radiation, the rapid evolution of ecological and phenotypic diversity within a clade, may account for much of life's diversity (*1*, *2*). The ecological theory of adaptive radiation is founded on the unifying concept of the adaptive landscape, the topographical relationship between fitness and a continuous phenotypic space (*1*). This theory predicts early bursts of niche diversification due to rapid invasion of multiple, unoccupied fitness peaks after colonization, the evolution of a key innovation, or mass extinction (*1*–*5*). This "early burst" model is supported by microbial evolution (*4*), the fossil record (*6*), and species diversification in some clades (*7*), but the pattern is rare in comparative data (*8*). Indeed, observations of disruptive selection suggest that many populations are constrained from ascending fitness peaks (*9*, *10*).

Most studies of selection estimate its local form—directional, stabilizing, or disruptive (*1*, *9*)—but few investigate the broader topography of the fitness surface, particularly among multiple species (*11*–*13*) or traits (*14*), or by manipulating phenotypes to measure the fitness of intermediates between species (*12*, *15*–*17*). However, measurement of the broader multivariate fitness landscape is necessary to demonstrate a local maximum and to visualize the selective surface during early bursts of niche diversification. Multipeak fitness landscapes have been demonstrated in laboratory microcosms (*4*) and inferred from resource availabilities (*18*), foraging performance (*13*), and mark-recapture (*11*) in the field, but not from fitness measurements of manipulated phenotypes. Thus, the key early burst prediction of multiple fitness peaks has never been experimentally tested in the wild.

Department of Evolution and Ecology and Center for Population Biology, University of California, One Shields Avenue, Davis, CA, USA

*To whom correspondence should be addressed. E-mail: chmartin@ucdavis.edu

We measured fitness landscapes directly from growth and survival of F_2 hybrids from crosses among the three species in a sympatric adaptive radiation of *Cyprinodon* pupfishes on San Salvador Island, Bahamas. F_2 hybrids spanned the range of morphological diversity represented in the three parental species. This small island radiation contains ecologically novel species and displays rapid morphological diversification rates similar to those of classic adaptive radiations (*19*), yet is less than 10,000 years old (*20*). The endemic radiation contains two trophic specialist species, a scale-eater and a hard-shelled–prey specialist (durophage), both novel ecological niches within *Cyprinodon*, and a third generalist species similar to the wide-ranging species *C. variegatus*. The three species co-occur in all habitats within the island's shallow saline lakes containing only two other fish species. Although generalist populations are ubiquitous across similar environments in the Caribbean with identical fish communities, the San Salvador clade is one of only two sympatric radiations of *Cyprinodon* and exhibits morphological diversification rates up to 51 times faster than those of other young clades for functional trophic traits (*19*).

We tested the effects of competition in the wild on the topography of fitness landscapes during *Cyprinodon* adaptive radiation by measuring the fitness of 1865 hybrids placed in high- and low-density field enclosures. Wild-caught breeding colonies of all three species were used to generate outbred F_2 hybrid populations for this experiment from F_1 hybrid intercrosses and backcrosses (*20*). Hybrid populations from two isolated lakes, Crescent Pond (CP) and Little Lake (LL), were generated independently. First, these laboratory-reared juvenile F_2 hybrids were measured for 16 morphological traits and implanted with coded wire tags. Next, we transported the hybrids to San Salvador Island and introduced them into a low- or high-density field enclosure in the respective lake from which their grandparents originated (CP: high/low-density n = 796/96 hybrids; LL: n = 875/98 hybrids). After 3 months, we recovered all surviving hybrids and assigned a fitness of 1 relative to 0 for unrecovered hybrids. Fitness was also estimated from the growth (the increase in standard length) of survivors in enclosures.

To provide a biologically relevant frame of reference for hybrid morphology, we laboratory-reared and measured a purebred F_1 generation of all three species from each lake. We then plotted the hybrids in a discriminant morphospace separating the F_1 purebred species in each lake and visualized fitness landscapes for survival (Fig. 1) and growth (fig. S1). Morphospace coverage was reduced in LL, probably due to missing a backcross to the durophage.

Fitness landscape topography was complex but largely congruent between high-density enclosures in each lake for both survival and growth (Fig. 1 and fig. S1). A local fitness peak in the high-density CP enclosure, isolated by declining fitness in all directions, corresponded to the phenotype of the generalist species (Fig. 1, A, C, and E). Phenotypic similarity between hybrids on this local fitness peak and the laboratory-reared generalist species cannot be attributed to familial relatedness or shared environments (*20*). Instead, this correspondence demonstrates strong stabilizing selection on hybrid phenotypes closely resembling generalists. There was a similar trend in LL (Table 1 and Fig. 2). Survival also declined with increasing total phenotypic distance from the generalist in both high-density enclosures (fig. S2).

A second region of increased fitness [linear discriminant axis 1 (LD1) < 0 and LD2 < 0 in Fig. 1A: n = 120 hybrids, logistic z-score = –2.33, P = 0.020] corresponded to the phenotype and the diet (inferred from $\delta^{15}N$ stable isotopes) of the hard-shelled–prey specialist (durophage; Figs. 1 and 2, figs. S3 and S4, and table S1). In the CP high-density enclosure, increased survival in this region was supported by parametric and permutation tests (*20*), although less strongly than the generalist peak. This fitness region was also significantly higher (permutation test, n = 796 hybrids, P = 0.044) than the generalist peak (Fig. 1E) and was robust to alternative calculations of the discriminant morphospace (figs. S5 and S6). A similar trend of increased survival of hybrids resembling the durophage specialist was observed in LL (Figs. 1 and 2 and Table 1). Furthermore, CP hybrid survivors in this region occupied a higher trophic position than those on the generalist peak ($\delta^{15}N$ stable isotope ratios: n = 64 hybrids, permutation test, P = 0.048; fig. S3 and table S1), reflecting the relative trophic positions of wild-caught durophage and generalist pupfishes ($F_{1,22}$ = 8.78, P = 0.007; table S1). Thus, trophic divergence between hybrids mirrored trophic divergence in wild-caught species.

Hybrids resembling generalist and durophage phenotypes were separated by a valley of reduced fitness in both lakes (Fig. 2). Transects between species indicated significant disruptive

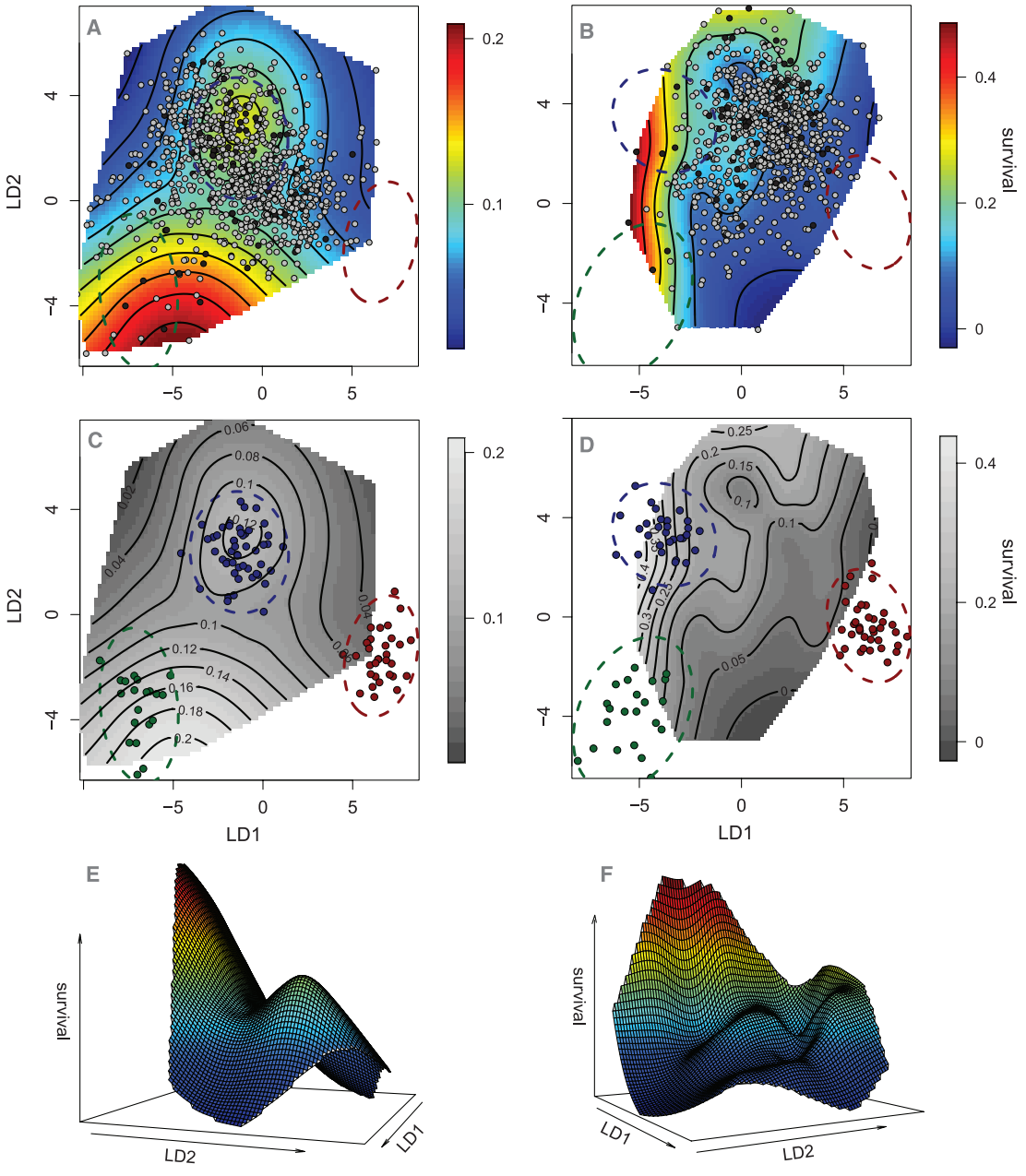

Fig. 1. Survival fitness landscape for F_2 hybrids within the high-density field enclosure in each lake (left column: CP; right column: LL). (**A** and **B**) Individual F_2 hybrid survivors (black dots) and deaths (gray dots) plotted within the discriminant morphospace (LD1 and LD2) estimated from laboratory-reared purebred species. Heat colors indicate survival probabilities estimated from thin-plate splines fit to the data by generalized cross-validation (effective df: CP, 7.6; LL, 19.6). (**C** and **D**) Laboratory-reared purebred species are superimposed within 95% confidence ellipses (dashed lines: generalist, blue dots; durophage, green dots; scale-eater, red dots) for reference. (**E** and **F**) Relative heights of the fitness landscape.

Table 1. Significance of local regions of stabilizing ($\gamma < 0$) and disruptive ($\gamma > 0$) selection within survival fitness landscapes for F_2 hybrids in high-density field enclosures (Fig. 1). The form of selection on hybrid phenotypes was tested for the quadratic intervals depicted in Fig. 2. Sample sizes within each interval are reported for each test. *n*, number of hybrids; GLM, generalized linear model.

Hybrid transect	Lake	Quadratic interval	γ	Survival		Growth		Joint†
				n	Logistic *P*	*n*	GLM *P*	Permutation *P*
Durophage versus generalist	CP	Fig. 2A (i)	−0.120	355	0.024*	46	0.963‡	0.006**
	LL	Fig. 2B (i)	−0.150	52	0.203	9	0.644	0.047*
	Combined							1.4×10^{-4}***
	CP	Fig. 2A (ii)	0.160	359	0.005**	52	0.050*	0.002**
	LL	Fig. 2B (ii)	0.432	27	0.030*	8	0.911	0.043*
	Combined							3×10^{-5}****
Generalist versus scale-eater	CP	Fig. 2C	−0.132	555	0.006**	64	0.734‡	0.001**
	LL	Fig. 2D	0.104	406	0.152	44	0.497‡	0.473

*$P < 0.05$, **$P < 0.01$, ***$P < 0.001$, ****$P < 0.0001$. †Joint significance of selection gradients (γ) for both growth and survival (*20*). ‡Survival and growth did not agree on the form of selection (opposite signs), and the joint test used only survival data. Selection gradients (γ) for survival are shown.

selection on intermediate phenotypes (Table 1, Fig. 2). The form of selection on growth was not always consistent with survival (Table 1); however, multiple regions of increased fitness, corresponding to generalist and durophage phenotypes, were observed in both survival and growth fitness landscapes in the high-density CP enclosure and showed a similar trend in LL (Fig. 1 and fig. S1).

Hybrids resembling the scale-eater phenotype had greatly reduced survival and growth in both lakes at high and low densities (Figs. 1 and 2, fig. S1, and Table 1), demonstrating that low fitness over a large region of morphospace reproductively isolates this species from the others. Hybrid survivors resembling scale-eaters rarely ingested any scales (4 out of 11 relative to 49 out of 53 wild-caught scale-eaters);

thus, scale-eating may require an extreme phenotype, not recovered in hybrids, for successful performance. Alternatively, field enclosures may not support the scale-eating niche; however, we consider this unlikely because the frequency of hybrids resembling scale-eaters within high-density enclosures (CP, 0.6%; LL, 0.9%) was similar to wild scale-eater frequencies [1.4% (*20*)], prey density was higher in enclosures, and fitness did not vary between density treatments. Overall, the reduced fitness of intermediate and transgressive hybrids supports the importance of postzygotic extrinsic reproductive isolation.

High-density enclosures provided a more competitive environment than low-density enclosures: Survival was 4 to 7 times higher and growth was 1.4 to 2 times higher in low-density enclosures (mean survival: CP, 11.4% versus 71.9%; LL, 11.1% versus 43.9%; logistic $z = 11.8$, $P < 10^{-16}$; mean growth: CP, 0.196 versus 0.428 cm; LL, 0.164 versus 0.223 cm; $t = -2.8$, $P = 0.005$). The curvature of the fitness landscape was significantly greater in high-density enclosures in both lakes (Table 2 and figs. S1 and S7), supporting competition as the driver of multiple fitness peaks on the adaptive landscape. If intrinsic differences in fitness among hybrid phenotypes were responsible, complex fitness landscapes should occur in both field and laboratory environments. However, laboratory survival surfaces, estimated from hybrids that died during laboratory rearing, were flat (table S2 and fig. S8). Combined, these data indicate that multiple high-fitness regions were caused by competition for diverse resources, not intrinsic survival differences.

This complex fitness landscape paints an intriguing picture of niche diversification driven by competition in *Cyprinodon*. The generalist species sits atop a local fitness maximum separated by a valley from a higher-fitness region corresponding to specialization on hard-shelled prey. Stabilizing selection on generalist phenotypes could explain the rarity of trophic specialists within *Cyprinodon* despite their higher fitness: Sympatric adaptive radiations of trophic specialists may have evolved in only two places throughout the Caribbean because most generalist populations are stranded on an isolated local maximum. When subpopulations escape this generalist peak, perhaps through increased competition, ecological opportunity, and large effective population size, the higher fitness of trophic specialists drives a burst of diversification.

The early burst model of adaptive radiation predicts a fitness landscape with multiple peaks at the onset of adaptive radiation (*1*, *2*, *4*, *7*, *8*). We simulated phenotypic diversity within the ancestral population that gave rise to an adaptive radiation of pupfishes in order to measure the initial topography of the fitness landscape. In contrast to theory and examples demonstrating that high-frequency phenotypes cause a fitness minimum due to negative frequency-dependent selection (*9*, *10*), some of the most frequent phenotypes in our field enclosures occurred on a local

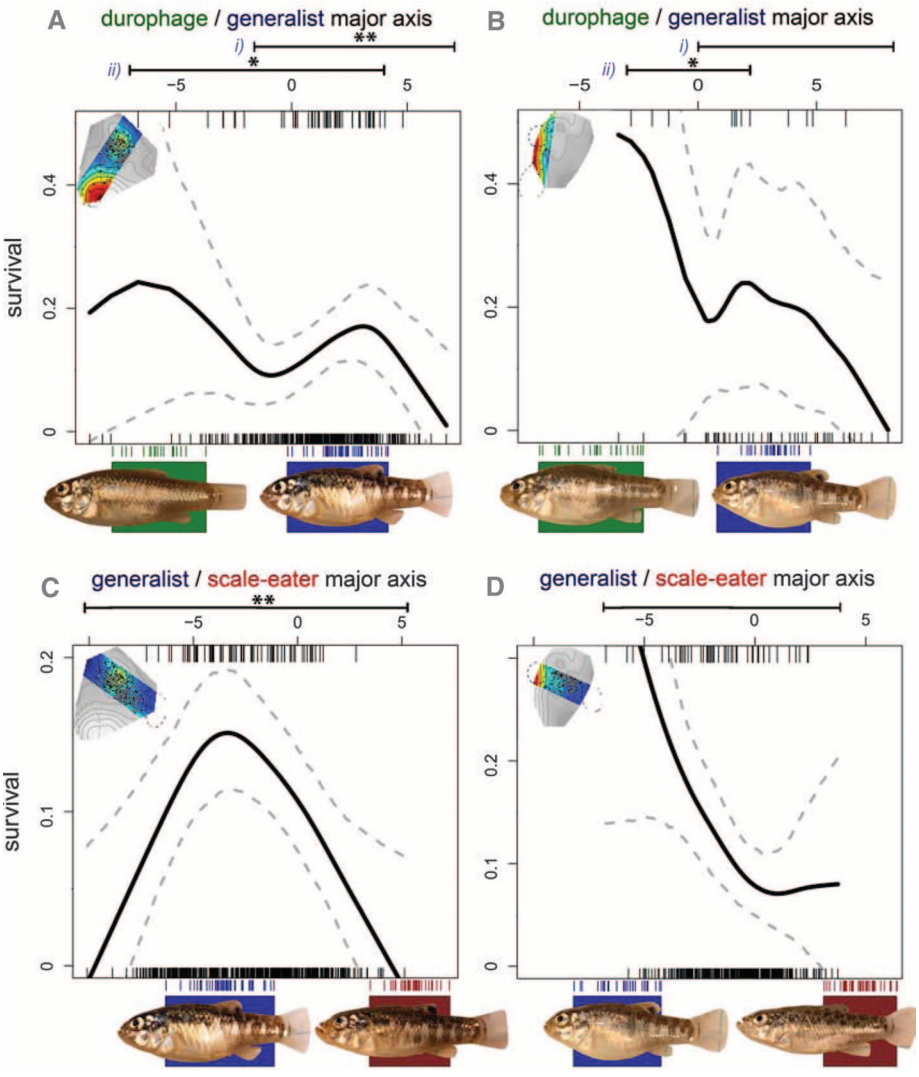

Fig. 2. Probability of F_2 hybrid survival in high-density field enclosures within local transects between species (left column, CP; right column, LL). Smoothing splines (black line) and 95% confidence intervals (dotted gray lines) indicate hybrid survival along major phenotypic axes between species ellipses from Fig. 1 (insets at upper left). (**A** and **B**) Major axis between hybrids resembling durophage or generalist species. (**C** and **D**) Major axis between hybrids resembling generalist or scale-eater species. Interior rug plots show F_2 hybrid survivors (upper) and deaths (lower). Exterior rug plots show laboratory-reared F_1 purebred species (generalist, blue; durophage, green; scale-eater, red) for reference. Quadratic intervals used for parametric analyses (Table 1) are indicated with significance from logistic regression.

Table 2. Effect of competition on fitness landscape curvature. Three permutation tests assessed the significance of greater survival surface curvature in high-density enclosures relative to low-density enclosures (fig. S7), controlling for different sample sizes and morphospace coverage. Significance was determined from the number of randomized samples equal to or greater than the observed difference between treatments (*20*). Effective degrees of freedom (EDF) indicate the smoothness of the surface estimated by generalized cross-validation.

Lake	Density	*n*	Thin-plate spline		Projection pursuit regression		Canonical rotation of γ	
			EDF	*P*	EDF	*P*	*F*	*P*
Crescent Pond	High	796	7.6	0.071•	3.1	0.065•	3.41	0.018*
	Low	96	3.0		2.0		0.01	
Little Lake	High	875	19.6	0.008**	6.7	0.006**	1.03	0.711
	Low	98	3.0		2.4		1.73	

•$P < 0.10$, *$P < 0.05$, **$P < 0.01$.

fitness maximum, suggesting that the broader topography of adaptive landscapes is more strongly determined by stable performance constraints than frequency-dependent dynamics.

References and Notes

1. D. Schluter, *The Ecology of Adaptive Radiation* (Oxford Univ. Press, Cambridge, 2000).
2. G. G. Simpson, *Tempo and Mode in Evolution* (Columbia Univ. Press, New York, 1944).
3. R. Lande, *Evolution* **33**, 402 (1979).
4. E. I. Svensson, R. Calsbeek, *The Adaptive Landscape in Evolutionary Biology* (Oxford Univ. Press, Oxford, 2012).
5. S. Wright, *Proc. VI Int. Cong. Gen.* **1**, 356 (1932).
6. M. Foote, *Annu. Rev. Ecol. Syst.* **28**, 129 (1997).
7. D. L. Rabosky, I. J. Lovette, *Proc. Biol. Sci.* **275**, 2363 (2008).
8. L. J. Harmon *et al.*, *Evolution* **64**, 2385 (2010).
9. J. G. Kingsolver *et al.*, *Am. Nat.* **157**, 245 (2001).
10. C. H. Martin, *Am. Nat.* **180**, E90 (2012).
11. A. P. Hendry, S. K. Huber, L. F. De León, A. Herrel, J. Podos, *Proc. Biol. Sci.* **276**, 753 (2009).
12. D. Schluter, *Science* **266**, 798 (1994).
13. C. W. Benkman, *Evolution* **57**, 1176 (2003).
14. R. Calsbeek, D. J. Irschick, *Evolution* **61**, 2493 (2007).
15. C. S. McBride, M. C. Singer, *PLoS Biol.* **8**, e1000529 (2010).
16. E. Svensson, B. Sinervo, *Evolution* **54**, 1396 (2000).
17. D. W. Schemske, H. D. Bradshaw Jr., *Proc. Natl. Acad. Sci. U.S.A.* **96**, 11910 (1999).
18. D. Schluter, P. R. Grant, *Am. Nat.* **123**, 175 (1984).
19. C. H. Martin, P. C. Wainwright, *Evolution* **65**, 2197 (2011).
20. Additional supporting data and analyses are available in the supplementary materials on *Science* Online.

Acknowledgments: Funded by NSF grant DDIG DEB-1010849, the Gerace Research Centre, and the Center for Population Biology. Permits were approved by the Bahamian government and the University of California, Davis. G. Mount and S. Romero assisted with research; T. Schoener, M. Turelli, A. Hendry, D. Nychka, L. Schmitz, and C. Boettiger provided feedback. C.H.M. designed the study, raised funding, performed research, collected and analyzed data, and wrote the paper. P.C.W. contributed materials, discussed design and results, and commented on the manuscript.

Supplementary Materials

www.sciencemag.org/cgi/content/full/339/6116/208/DC1
Materials and Methods
Figs. S1 to S9
Tables S1 to S9
References (*21*–*51*)

20 July 2012; accepted 16 November 2012
10.1126/science.1227710

Suppression of Oxidative Stress by β-Hydroxybutyrate, an Endogenous Histone Deacetylase Inhibitor

Tadahiro Shimazu,[1,2] Matthew D. Hirschey,[1,2] John Newman,[1,2] Wenjuan He,[1,2] Kotaro Shirakawa,[1,2] Natacha Le Moan,[3] Carrie A. Grueter,[4,5] Hyungwook Lim,[1,2] Laura R. Saunders,[1,2] Robert D. Stevens,[6] Christopher B. Newgard,[6] Robert V. Farese Jr.,[2,4,5] Rafael de Cabo,[7] Scott Ulrich,[8] Katerina Akassoglou,[3] Eric Verdin[1,2]*

Concentrations of acetyl–coenzyme A and nicotinamide adenine dinucleotide (NAD^+) affect histone acetylation and thereby couple cellular metabolic status and transcriptional regulation. We report that the ketone body D-β-hydroxybutyrate (βOHB) is an endogenous and specific inhibitor of class I histone deacetylases (HDACs). Administration of exogenous βOHB, or fasting or calorie restriction, two conditions associated with increased βOHB abundance, all increased global histone acetylation in mouse tissues. Inhibition of HDAC by βOHB was correlated with global changes in transcription, including that of the genes encoding oxidative stress resistance factors FOXO3A and MT2. Treatment of cells with βOHB increased histone acetylation at the *Foxo3a* and *Mt2* promoters, and both genes were activated by selective depletion of HDAC1 and HDAC2. Consistent with increased FOXO3A and MT2 activity, treatment of mice with βOHB conferred substantial protection against oxidative stress.

Cellular metabolites such as acetyl–coenzyme A (acetyl-CoA) and nicotinamide adenine dinucleotide (NAD^+) influence gene expression by serving as cofactors for epigenetic modifiers that mediate posttranslational modification of histones (*1*). The activity of histone acetyltransferases (HATs) is dependent on nuclear acetyl-CoA concentrations (*2*, *3*) and the deacetylase activity of class III HDACs, also called sirtuins, is dependent on NAD^+ concentrations (*4*). Class I (HDAC1, 2, 3, 8), class II (HDAC4, 5, 6, 7, 9, 10), and class IV (HDAC11) HDACs are zinc-dependent enzymes, but endogenous regulators are not known.

Small-molecule inhibitors of class I and class II HDACs include butyrate, a product of bacterial anaerobic fermentation (*5*). Butyrate is closely related to β-hydroxybutyrate (βOHB) (Fig. 1A), the major source of energy for mammals during prolonged exercise or starvation (*6*). Accumulation of βOHB in blood increases to 1 to 2 mM during fasting when the liver switches to fatty acid oxidation (*7*, *8*), and to even higher concentrations during prolonged fasting (6 to 8 mM) (*6*) or in diabetic ketoacidosis (>25 mM) (*9*).

To determine whether βOHB might have HDAC inhibitor activity, we treated human embryonic kidney 293 (HEK293) cells with different amounts of βOHB for 8 hours, and measured histone acetylation levels by Western blot with antibodies to acetylated histone H3 lysine 9 ($AcH3_{K9}$) and to acetylated histone H3 lysine 14 ($AcH3_{K14}$) (Fig. 1, B and C, and figs. S1 and S2). βOHB increased histone acetylation in a dose-dependent manner, even at 1 to 2 mM, which can occur in humans after a 2- to 3-day fast or strenuous exercise (*6*, *8*, *10*). Like butyrate, βOHB did not increase acetylation of α-tubulin, indicating that it inhibits class I HDACs but not the class IIb tubulin deacetylase, HDAC6.

To test the HDAC inhibitor activity of βOHB and its possible selectivity, we purified recombinant human HDACs after transient transfection of expression vectors for human epitope-tagged (FLAG) HDAC1, HDAC3, HDAC4, and HDAC6 in HEK293T cells. We purified the HDACs, incubated them with ^3H-labeled acetylated histone H4 peptides, and measured their deacetylase activity (Fig. 1D) (*11*). βOHB inhibited HDAC1, HDAC3, and HDAC4 in a dose-dependent manner with a median inhibitory concentration (IC_{50}) of 5.3, 2.4, and 4.5 mM, respectively. The HDAC6 IC_{50} was much higher (48.5 mM) (Fig. 1E), and βOHB did not inhibit HDAC6 activity on its natural substrate tubulin (fig. S3). To examine the possibility that histone acetylation was enhanced by increased concentration of acetyl-CoA (because βOHB is catabolized into acetyl-CoA in target tissues), we directly measured abundance of acetyl-CoA in βOHB-treated HEK293 cells, but no change was observed (fig. S4). We also tested a possible activating effect of βOHB on histone acetyltransferase activity of p300 and PCAF (P300/CBP-associated factor) but did not detect any change induced by βOHB (fig. S5). Thus, millimolar concentrations of βOHB appear to increase histone acetylation directly through HDAC inhibition. High concentrations of acetoacetate (AcAc) also inhibit class I and class IIa HDACs in vitro (fig. S6A) and in HEK293 cells (fig. S6B). However, the concentration of AcAc in blood is one-third or less than that of βOHB during fasting and therefore less likely to reach concentrations that would inhibit HDACs under physiological conditions (*12*). To test the relative contribution of βOHB,

[1]Gladstone Institute of Virology and Immunology, San Francisco, CA 94158, USA. [2]Department of Medicine, University of California, San Francisco, CA 94143, USA. [3]Gladstone Institute of Neurological Disease, San Francisco, CA 94158, USA. [4]Gladstone Institute of Cardiovascular Disease, San Francisco, CA 94158, USA. [5]Department of Biochemistry and Biophysics, University of California, San Francisco, CA 94143, USA. [6]Sarah W. Stedman Nutrition and Metabolism Center, and Departments of Pharmacology and Cancer Biology and Medicine, Duke University Medical Center, Durham, NC 27704, USA. [7]Laboratory of Experimental Gerontology, National Institute on Aging, National Institutes of Health, Baltimore, MD 21224, USA. [8]Department of Chemistry, Ithaca College, Ithaca, NY 14850, USA.

*To whom correspondence should be addressed. E-mail: everdin@gladstone.ucsf.edu